

Effective Hamiltonian approach to the exact dynamics of open system by complex discretization approximation for environment

H. T. Cui ^{1,*}, Y. A. Yan ^{1,†}, M. Qin ^{1,‡} and X. X. Yi ^{2§}

¹ *School of Physics and Optoelectronic Engineering & Institute of Theoretical Physics, Ludong University, Yantai 264025, China and*

² *Center for Quantum Sciences, Northeast Normal University, Changchun 130024, China*

(Dated: May 28, 2024)

The discretization approximation method commonly used to simulate the open dynamics of system coupled to the environment in continuum often suffers from the recurrence. To address this issue, this paper proposes a novel generalization of the discretization approximation method in the complex plane using complex Gauss quadratures. The effective Hamiltonian can be constructed by this way, which is non-Hermitian and demonstrates the complex energy modes with negative imaginary part, describing accurately the dissipative dynamics of the system. This method is applied to examine the dynamics in two exactly solvable models: the dephasing model and the single-excitation open dynamics in the Aubry-André-Harper model. This approach not only significantly reduces recurrence and improve the effectiveness of calculation, but also provide the microscopic viewpoint on the dynamics of system through the effective Hamiltonian. In addition, a simple relationship between the parameters in computation and the effectiveness of evaluation is also established.

I. INTRODUCTION

A quantum system is inherently connected to its surroundings, which can lead to equilibrium or nonequilibrium. However, rigorous numerical or analytical description of the open quantum systems appears to be extremely difficult as one has to deal with large or infinite number of environmental degrees of freedom. Hence, assumptions such as the weak system-environment coupling and vanishing correlation times of the environment, known as Born-Markov approximation, are usually invoked to find compact and solvable equations [1]. These approaches sacrifice the accuracy for the sake of operability and may become incorrect in some circumstances. Indeed, recent experimental advances have demonstrated the instances that cannot be formulated under the Born-Markov approximation, such as in solid-state and artificial light-matter systems [3], as well as in quantum biology and chemistry [4]. In certain situations, nonequilibrium dynamics have also been observed, which demonstrate the importance of the system's dynamics in relation to the non-Markovianity or memory effect of environment [5, 6]. Thus, it is crucial for the research of open dynamics of system to take the property of environment into account completely.

Simulating the open quantum systems imposes a theoretical challenge when the influence of environment is incorporated completely, often requiring the use of perturbation expansion or numerical simulation [7]. One common approach is to employ projection operator techniques [1], which can yield the Nakjima-Zwanzig equation [8] or the time-convolutionless master equation [9]. These

equations can be used to derive effective master equations through perturbational expansion based on the strength of the system-environment coupling. Numerical simulations, such as stochastic Schrödinger equations [10], hierarchical equations of motion [11], path integral methods [12], and tensor networks [13], have also been proposed to determine the open dynamics of system. These methods involve introducing an influence functional to characterize the environmental effect on the system, thereby eliminating the degree of freedom of the environment from the dynamical equation.

An alternative method for studying open quantum systems involves incorporating the complete dynamics of both the system and its surrounding environments [14]. Under the limit of infinite degree of freedom in environments, the Hamiltonian and coupling to the system can be represented as the integrals. Consequently, orthogonal polynomials can be applied to discretize the integrals, resulting in a chain representation of the total Hamiltonian. This approach enables the use of powerful numerical techniques to evaluate the full dynamics, and its efficiency and convergence have been demonstrated clearly [15]. Compared to the previous methods, this approach allows for the explicit determination of the eigenfunctions of the chain Hamiltonian, thereby revealing the microscopic properties of the dynamics.

However, the recurrence resulting from the finite dimension of chain Hamiltonian can negatively impact the effectiveness and accuracy of discretization approximation. To address this issue, an effective approach is to extend the discretization approximation into the complex plane, resulting in the emergence of complex energy levels that represent dissipation in systems. This concept was initially proposed to examine resonance decay in systems with a discrete state connected to a continuum [16]. The approach involves discretizing integrals in dynamical equations using Gauss quadrature rules to obtain finite summations of complex items. This results in dynamical

* cuiht01335@aliyun.com

† yunan@ldu.edu.cn

‡ qinming@ldu.edu.cn

§ yixx@nenu.edu.cn

equations that can efficiently simulate decay dynamics due to the occurrence of pseudostates with complex energies. However, this approach is highly specific and may not be applicable in more general situations.

In this paper, a complex generalization of the discretization approximation for the environment is presented from a fundamental perspective. The approach involves introducing orthonormalized polynomials in the complex plane and applying a unitary transformation to achieve the discretization. The resulting effective full Hamiltonian is non-Hermitian, and thus possess the complex energy modes with negative imaginary part, which accurately describe the dissipative dynamics in the system. It is demonstrated by two exactly solvable models that this effective Hamiltonian can provide the excellent simulation for the open dynamics of the system. The paper is divided into six sections, starting with a general description of the system and environment in Section II. Section III explains how to expand the discretization approximation into the complex plane, with a focus on the introduction of the complex orthonormalized polynomials by the contour integrals in the complex plane. The method is illustrated for two exactly solvable model in section IV: the dephasing model and the open dynamics of the Aubry-André-Harper model (AAH) in the single-excitation subspace. The error in computation is analyzed explicitly in section V, where a simple relation between the parameters of calculation and the evolution time t can be established. Finally, conclusions and a discussion are given at the end of paper.

II. GENERAL DESCRIPTION OF THE OPEN QUANTUM SYSTEM

It is convenient to model the environment as a structureless system with a large number of degree of freedom. To be precise, the dynamics of the system and environment can be explicated by the total Hamiltonian below:

$$\begin{aligned} H &= H_s + H_b + H_{int} \\ H_b &= \sum_k \omega_k b_k^\dagger b_k; \\ H_{int} &= \sum_{n,k} \left[g_k c_n^\dagger b_k + g_k^* b_k^\dagger c_n \right], \end{aligned} \quad (1)$$

in which c_n or the Hermitian conjugation c_n^\dagger represents the lowering or raising operator in the system. b_k^\dagger, b_k is creation or annihilation operator of the k -th mode in environment. In this paper, we focus only on the bosonic environment. Thus the bosonic commutative relations

$$\left[b_k, b_{k'}^\dagger \right] = \delta_{k,k'}$$

are imposed. Without loss of the generality, it is posited that the Hamiltonian of the system, denoted by H_s , can be expressed in a matrix form, with the subscript n denoting the distinct degree of freedom within the system.

The environment is described as a set of independent frequency modes, labelled by subscript k . The coupling between the system and environment is represented by H_{int} , with the coupling strength being depicted by g_k or its complex conjugation g_k^* . The rotating-wave approximation has been applied to ensure that the total number of excitations is conserved. As for the large number of degree of freedom in environment, it is convenient to character the interaction by the spectral function $J(x)$ defined as

$$J(x) = \sum_k |g_k|^2 \delta(x - \omega_k). \quad (2)$$

Thus, in the limit $k \rightarrow \infty$ and the frequency representation $g_k \rightarrow g(x)$, $J(x)$ may be written in the continuum as [17]

$$J(x) = g^2 [h^{-1}(x)] \frac{dh^{-1}(x)}{dx}, \quad (3)$$

where $h^{-1}(x)$ is the inverse of the dispersion relation $h(x)$ and $\frac{dh^{-1}(x)}{dx}$ represents the density of state of environment in frequency space. In this sense, one can relate the frequency ω_k to the variable x . By this transformatin, H_b and H_{int} can be expressed equivalently as

$$\begin{aligned} H_b &\Rightarrow \int_0^\infty dx h(x) b_x^\dagger b_x; \\ H_{int} &\Rightarrow \sum_n \int_0^\infty dx [g(x) c_n^\dagger b_x + g^*(x) b_x^\dagger c_n], \end{aligned} \quad (4)$$

As a consequence, $\left[b_x, b_{x'}^\dagger \right] = \delta(x - x')$ is a natural requirement such that $\int dx \left[b_x, b_{x'}^\dagger \right] = \sum_k \left[b_k, b_{k'}^\dagger \right] = 1$ must be satisfied.

It is noteworthy that the functions $h(x)$ or $g(x)$ are not uniquely determined for a given $J(x)$. By this freedom, one can choose proper form for $h(x)$ or $g(x)$ for the sake of discretization of environment [14]. Given Ohmic spectral function

$$J(x) = \eta x \left(\frac{x}{\omega_c} \right)^{s-1} e^{-x/\omega_c}, \quad (5)$$

one may choose

$$h(x) = \omega_c x, g(x) = \sqrt{\eta} \omega_c x^{s/2} e^{-x/2}. \quad (6)$$

Assuming that $h(x)$ has a linear relationship with variable x is beneficial to the discretization of environment. In Appendix I, a brief overview of the discretization approximation method in real space is outlined, and then is applied to simulate the open dynamics in two exactly solvable models. It is illustrated that the simulation is hampered by recurrence, consequently making the calculation ineffective.

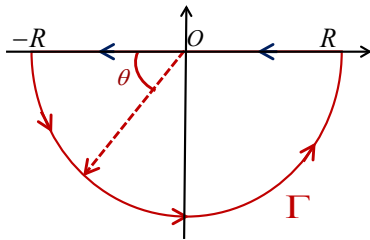


Figure 1. (Color online) The diagrammatic sketch of integral path in the inner product defined by Eq. (7). The red solid line, labelled by Γ , denotes a semicircle with radius R on the lower half of complex plane.

III. COMPLEX GAUSS QUADRATURES AND CHAIN-MAPPING IN COMPLEX PLANE

To reduce the recurrence, we extend the discretization approximation into the complex space in this section. Similar to the procedure shown in Appendix I, the first step is to find the complex Gauss quadratures.

A. Complex Gauss Quadratures

In order to extend the Gauss quadratures to the complex plane, it is necessary to transform the integral in real space into a contour integration in the complex plane. For this purpose, a contour in the lower half of complex plane, as sketched in Fig. 1, is chosen in accordance with the method presented in Refs. [19]. This choice is crucial to obtain a unique set of complex polynomials with zero points that exhibits negative imaginary part. In convenience of discussion, $R = 1$ is assumed in the following discussion. Thus, $z = e^{i\theta}$.

The inner product for complex polynomials $f(z)$ and $g(z)$ is defined as the integral along contour Γ [19],

$$\langle f, g \rangle_{\Gamma} = \int_{\Gamma} \frac{dz}{iz} w(z) f(z) g(z) = \int_{\pi}^{2\pi} d\theta w(e^{i\theta}) f(e^{i\theta}) g(e^{i\theta}), \quad (7)$$

where Γ denotes the integral path as a semicircle with radius R on the lower half of complex plane, as shown by red solid line in Fig. 1. For weight function $w(z)$, $\text{Re} \int_{\pi}^{2\pi} d\theta w(e^{i\theta}) \neq 0$ is required such that the zero point of the determined polynomial displays nonvanishing imaginary part. It is emphasized that the inner product is defined deliberately without complex conjugation. Only by this way, the three-term recurrence relation can be constructed since $\langle zf, g \rangle_{\Gamma} = \langle f, zg \rangle_{\Gamma}$ is satisfied [19]. Importantly, we stress that $\langle f, f \rangle_{\Gamma}$ does not correspond to the norm of $f(z)$ as it may be complex or even zero by Eq. (7). In another point, to construct the system of orthonormalized polynomials $\{\eta_n(z), n = 0, 1, 2, \dots\}$ where n denotes the degree of polynomials, $\langle \eta_n, \eta_m \rangle_{\Gamma} \neq 0$ must be required. Fortunately, it has been demonstrated in Ref. [19] that there is the one-to-one correspondence

between $\{\eta_n(z)\}$ and its real counterpart, constructed relative to the inner product $\int_{-1}^1 dx w(x) f(x) g(x)$. Thus, $\langle \eta_n, \eta_m \rangle_{\Gamma} \neq 0$ is the natural result of this correspondence. Actually, it also provides an alternative way to determine $\eta_n(z)$. Consequently, one can always find the system of complex polynomials $\{\eta_n(z), n = 0, 1, 2, \dots\}$ by Eq.(7), which satisfy the orthonormality

$$\langle \eta_m, \eta_n \rangle_{\Gamma} = \int_{\pi}^{2\pi} d\theta w(e^{i\theta}) \eta_m(e^{i\theta}) \eta_n(e^{i\theta}) = \delta_{m,n}. \quad (8)$$

Through Eq. (8), the following recurrence relation can be derived,

$$\sqrt{\nu_{n+1}} \eta_{n+1}(z) = (z - i\mu_n) \eta_n(z) - \sqrt{\nu_n} \eta_{n-1}(z), \quad (9)$$

where

$$i\mu_n = \langle z\eta_n, \eta_n \rangle_{\Gamma}, \nu_n = \frac{A_{n-1}^2}{A_n^2}, \quad (10)$$

A_n denotes the coefficient of z^n in $\eta_n(z)$. Alternatively, Eq. (9) can be represented in matrix form

$$z \begin{pmatrix} \eta_0 \\ \eta_1 \\ \vdots \\ \eta_{n-1} \end{pmatrix} = M_c \begin{pmatrix} \eta_0 \\ \eta_1 \\ \vdots \\ \eta_{n-1} \end{pmatrix} + \sqrt{\nu_n} \begin{pmatrix} 0 \\ 0 \\ \vdots \\ \eta_n \end{pmatrix};$$

$$M_c = \begin{pmatrix} i\mu_0 & \sqrt{\nu_1} & 0 & \cdots \\ \sqrt{\nu_1} & i\mu_1 & \ddots & 0 \\ 0 & \ddots & \ddots & \sqrt{\nu_{n-1}} \\ 0 & \cdots & \sqrt{\nu_{n-1}} & i\mu_{n-1} \end{pmatrix}. \quad (11)$$

By this matrix form, the zero points z_i and the corresponding weight w_i for $\eta_n(z)$ can be determined by solving eigenvalues and corresponding eigenfunctions of M_c . Noting that M_c is complex symmetric, the right and left eigenfunctions have relation $|i\rangle_R = (|i\rangle_L)^*$ ($i = 0, 1, 2, \dots, n-1$). By the similar method shown in Appendix I, one gets

$$w_i = [q_0^{(i)}]^2 \int_{\pi}^{2\pi} d\theta w(e^{i\theta}). \quad (12)$$

where $q_0^{(i)}$ denotes the first element of $|i\rangle_R$ for zero point z_i . It can be proved that z_i is confined in the region bounded by Γ and x -axis [18]. With these results, the following relation can be constructed

$$\int_{\Gamma} \frac{dz}{iz} w(z) f(z) \simeq \sum_i w_i f(z_i), \quad (13)$$

that is the generalization of Theorem 1 in Appendix I into the complex plane [19].

B. Mapping to the chain form

By Cauchy's integral theorem, one gets for any analytic function $f(z)$

$$\begin{aligned} \int_C dz f(z) &= \int_{\Gamma} dz f(z) - \int_{-R}^R dx f(x) = 0 \\ \therefore \int_{-R}^R dx f(x) &= \int_{\Gamma} dz f(z). \end{aligned} \quad (14)$$

where C denotes close path depicted by the arrows in Fig. 1. Thus, one can replace $\int_{-R}^R dx$ by $\int_{\Gamma} dz$. Correspondingly, the H_b and H_{int} in Eq.(4) can be rewritten as

$$\begin{aligned} H_b &= \int_{\Gamma} dz h(z) b_z^{\dagger} b_z; \\ H_{\text{int}} &= \int_{\Gamma} dz [g(z) c_n^{\dagger} b_z + g^*(z) c_n b_z^{\dagger}] \end{aligned} \quad (15)$$

Furthermore, b_x^{\dagger}, b_x is replaced by b_z^{\dagger}, b_z , and the commutative relation becomes $[b_z, b_{z'}^{\dagger}] = \delta(z - z')$.

Similar to the way adopted in Appendix I, we first introduce the transformation

$$\begin{aligned} d_n &= \int_{\Gamma} dz \sqrt{\frac{w(z)}{iz}} \eta_n(z) b_z \\ d_n^{\dagger} &= \int_{\Gamma} dz \sqrt{\frac{w(z)}{iz}} \eta_n(z) b_z^{\dagger} \end{aligned} \quad (16)$$

and the inverse

$$\begin{aligned} b_z &= \sqrt{\frac{w(z)}{iz}} \sum_{n=0}^{N_k-1} \eta_n(z) d_n \\ b_z^{\dagger} &= \sqrt{\frac{w(z)}{iz}} \sum_{n=0}^{N_k-1} \eta_n(z) d_n^{\dagger}. \end{aligned} \quad (17)$$

where N_k denotes the degree of polynomial in the discretization. It should be stressed that d_n^{\dagger} is not the Hermitian conjugation of d_n . Thus by Eq. (8). it is easy to prove

$$\begin{aligned} [d_n, d_m^{\dagger}] &= \iint dz dz' \sqrt{\frac{w(z)w(z')}{izzz'}} \eta_m(z) \eta_n(z') [b_z, b_{z'}^{\dagger}] \\ &= \int dz \frac{w(z)}{iz} \eta_m(z) \eta_n(z) = \delta_{m,n}. \end{aligned} \quad (18)$$

Specially, it should be pointed out the transformation in Eqs. (17) is unitary only if N_k is infinite. This effect of finite N_k is responsible for the computational errors.

Substituting Eqs. (17) into Eqs.15, one obtains respectively

$$H_b = \omega_c \sum_{i,j} d_i^{\dagger} d_j \int_{\Gamma} dz \frac{w(z)}{iz} z \eta_i(z) \eta_j(z). \quad (19)$$

Replacing $z \eta_i(z)$ by rearranging Eq. (9) and using Eq. (8), one gets

$$H_b = \omega_c (\cdots, d_m^{\dagger}, \cdots) M_c \begin{pmatrix} \vdots \\ d_n \\ \vdots \end{pmatrix}, \quad (20)$$

in which M_c is defined by Eq. (11). Apparently, the eigenvalues of M_c correspond to the discrete modes in environment, which is complex due to the non Hermiticity of M_c . Defining the new mode operator

$$\begin{aligned} \tilde{d}_i &= \sqrt{w_i} \sum_{n=0}^{N_k-1} \eta_n(z_i) d_n, \\ \tilde{d}_i^{\dagger} &= \sqrt{w_i} \sum_{n=0}^{N_k-1} \eta_n(z_i) d_n^{\dagger}, \end{aligned} \quad (21)$$

H_b then can be diagonalized as

$$H_b = \omega_c \sum_{i=0}^{N_k-1} z_i \tilde{d}_i^{\dagger} \tilde{d}_i. \quad (22)$$

As for H_{int} , one gets

$$H_{\text{int}} = \sum_{n=1}^{N_s} \sum_{i=0}^{N_k-1} \int_{\Gamma} dz \sqrt{\frac{w(z)}{iz}} \eta_i(z) [g(z) c_n^{\dagger} d_i + g^*(z) d_i^{\dagger} c_n] \quad (23)$$

in which $g(z)$ is the generalization of $g(x)$ in the complex plane.

C. Simplification of H_{int}

To simplify Eq. (23) further, one has to deal with the integration. It appears that $\int_{\Gamma} dz \sqrt{\frac{w(z)}{iz}} \eta_i(z) g(z)$ could be evaluated numerically only if $\eta_i(z)$ is determined. However, our empirical analysis has revealed that this methodology is not feasible. Instead, the right way is to approximate the integration according to Eq. (13) as

$$\begin{aligned} \int_{\Gamma} dz \sqrt{\frac{w(z)}{iz}} \eta_i(z) g(z) &= \int_{\Gamma} dz \frac{w(z)}{iz} \sqrt{\frac{iz}{w(z)}} \eta_i(z) g(z) \\ &\simeq \sum_{j=0}^{N_k-1} \sqrt{\frac{iz_j}{w(z_j)}} w_j \eta_i(z_j) g(z_j) \end{aligned} \quad (24)$$

Then, the first term in Eq.(23) is transformed into

$$\begin{aligned} &\sum_{n=1}^{N_s} \sum_{i,j=0}^{N_k-1} \sqrt{\frac{iz_j}{w(z_j)}} w_j \eta_i(z_j) g(z_j) c_n^{\dagger} d_i \\ &= \sum_n \sum_{j=0}^{N_k-1} \sqrt{\frac{iz_j}{w(z_j)}} \sqrt{w_j} g(z_j) c_n^{\dagger} \tilde{d}_j \end{aligned} \quad (25)$$

where the second equality comes from Eq. (21).

However, this approach encounters discrepancy when it is applied for $\int_{\Gamma} dz \sqrt{\frac{w(z)}{iz}} \eta_i(z) g^*(z)$. It comes from the observation that $g^*(z)$ actually equals to $g(z^*)$ by Eq. (6). As a result, it becomes problematic that one would discretize the integrals by Eq. (13), as both $\eta_i(z)$ and w_i are connected with z_i with negative imaginary part, rather than the conjugation z_i^* . To eliminate this discrepancy, it is natural to replace the second term in Eq. (23) with the complex conjugate of the first term. Accordingly, H_{int} can be approximated as

$$\begin{aligned} H_{\text{int}} &\simeq \sum_n^{N_s} \sum_{j=0}^{N_k-1} \left[\sqrt{\frac{iz_j}{w(z_j)}} \sqrt{w_j} g(z_j) c_n^\dagger \tilde{d}_j + \text{h. c.} \right] \\ &= \sum_n^{N_s} \sum_{j=0}^{N_k-1} \left(g_j c_n^\dagger \tilde{d}_j + \text{h. c.} \right) \end{aligned} \quad (26)$$

where $g_j = \sqrt{\frac{iz_j}{w(z_j)}} \sqrt{w_j} g(z_j)$. The correctness of the way has been examined by the illustrations in IV.

D. Evaluation of the full dynamics

In the case of an Ohmic environment, where x falls within the interval $[0, \infty)$, it is necessary to perform a translation of z_j to $R(1 + z_j)$. This ensures that the real part of $R(1 + z_j)$ corresponds to the value of x . Under this translation, one has

$$\begin{aligned} z_j &\rightarrow R(1 + z_j) \\ g_j &\rightarrow \sqrt{\frac{iRz_j}{w[R(1 + z_j)]}} \sqrt{w_j} g[R(1 + z_j)], \end{aligned} \quad (27)$$

The iRz_j is a result of the requirement that $\int_{\Gamma} \frac{dz}{iz} = \int_{\pi}^{2\pi} d\theta$ must be preserved under the translation. The precision of numerical evaluation is strongly relevant to the value of R since it determines the upper bound of integration.

Consequently, a non-Hermitian effective Hamiltonian, labelled by H_{eff} , can be obtained to evaluate the full dynamics of system plus environment. The eigenfunctions of H_{eff} satisfy the biorthonormality [20],

$${}_L \langle m | n \rangle_R = \delta_{m,n}, \quad (28)$$

where $|n\rangle_R$ denotes the right eigenfunction of H_{eff} with eigenvalue E_n , and $|n\rangle_L$ denotes the left eigenfunction with eigenvalue E_n^* . By solving the Schrödinger equation, the state $|\psi(t)\rangle$ of full system at any time t can be expressed as

$$|\psi(t)\rangle = \sum_n e^{-iE_n t} |n\rangle_{RL} \langle n | \psi(0) \rangle. \quad (29)$$

E. Simulating the stable or stretched dynamics of system

The effective Hamiltonian, H_{eff} , is expected to accurately model the dissipative dynamics of the system. The is because the complex eigenvalue E_n possesses the negative imaginary part, causing the amplitude in Eq. (29) to decay exponentially. In another point, the strong coupling between system and environment may lead to the nonequilibrium behavior, such as the stable oscillation between energy states or reaching a steady state apart from the equilibrium [3], or exhibiting stable behavior after a very long-time evolution known as the stretched dynamics. To capture these unique dynamics of system more accurately, the improvement for the previous evaluation is required.

After the explicit calculation, it is observed that replacing the expected E with its real part in Eq. (29) can result in an excellent simulation for the stable dynamics of system, i.e., utilizing

$$|\psi(t)\rangle = \sum_n e^{-i\text{Re}(E_n)t} |n\rangle_{RL} \langle n | \psi(0) \rangle. \quad (30)$$

The effectiveness of this method is examined thoroughly in Appendix IV, compared with the approach by Eq. (29) and the exact numerics, as well as the analytical approach. Admittedly, this proposition is empirical since it is aimed to recover the coherent evolution of system only by eliminating the exponential decaying of the amplitude. Regarding the stretched dynamics of system presented in the following section, our calculation shows that while Eq.(30) can provide the accurate simulation of the dynamics for a short-term evolution, it appears to be inadequate for predicating the long-term behavior.

With these preparations, we are ready to simulate the dynamics in the dephasing model and the open AAH model in the single-excitation subspace. It will be shown that depending on the status of system, the dynamics of system can displays the decaying, the stable oscillation or the stretched behavior, which can be captured rightly by the method proposed in this section.

IV. EXEMPLIFICATIONS

To ensure effective simulation, it is essential to choose $w(z)$ properly. The explicit calculation indicates that the choice of $w(z)/iz = \eta\omega_c^2 z^s e^{-z}$ is not suitable, since it leads to a real symmetric M_c . Resultantly, the eigenvalues of H_{eff} are real, which cannot improve the simulation. To eliminate this defect, we choose $w(z) = 1$ in the following discussion. As shown in the following illustrates, the simulation can be significantly improved, compared to the real case presented in Appendix I,

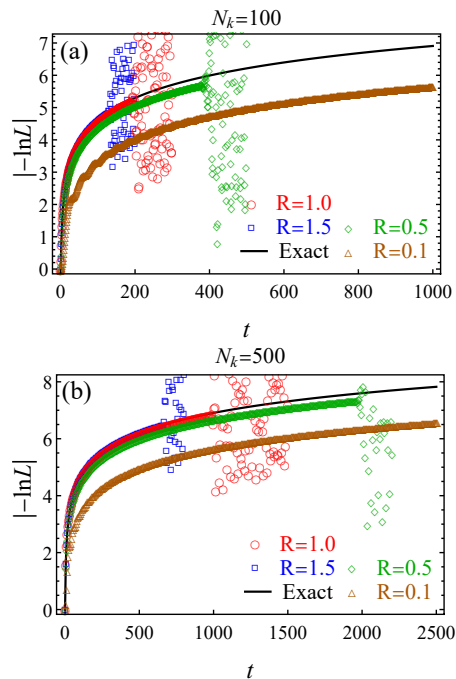


Figure 2. (Color online) The plots of the modulus of $-\ln L$ defined in Eq. (34) for different R and N_k . $\eta = \omega_c = 1$ is chosen for the plotting. The solid black line is obtained by Eq. (33). The evolution time t is in units of $1/\omega_c$.

A. Model I: the Dephasing model

The total hamiltonian is written as [1]

$$H = \frac{\omega_0}{2} \sigma_z + \sum_k \omega_k b_k^\dagger b_k + \frac{\sigma_z}{2} \sum_k (g_k b_k^\dagger + g_k^* b_k). \quad (31)$$

in which σ_z denotes the z component of Pauli operator, and b_k^\dagger, b_k are creation or annihilation operator of the k -th mode in the bosonic environment. It was known that the decoherence factor $L(t)$ at zero temperature is [1]

$$-\ln L = \sum_k |g_k|^2 \frac{1 - \cos \omega_k t}{\omega_k^2} = \int_0^\infty dx J(x) \frac{1 - \cos xt}{x^2} \quad (32)$$

Choosing Ohmic spectral density Eq. (5) and setting $\eta = \omega_c = 1$, one obtains for $s = 1$

$$-\ln L = \frac{1}{2} \ln(1 + t^2). \quad (33)$$

As for the complex discretization approximation, one may replace ω_k and g_k by z_j and g_j respectively. Thus, one has

$$-\ln L = \sum_j \left| \sqrt{\frac{iRz_j}{w[R(1+z_j)]}} \sqrt{w_j g [R(1+z_j)]} \right|^2 \times \frac{1 - \cos R(1+z_j)t}{R^2(1+z_j)^2}, \quad (34)$$

for which the translation Eq. (27) is used. Since $-\ln L$ becomes complex after this transformation, the modulus of $-\ln L$ is illustrated in Fig. 2. In comparison with the evaluation in real space illustrated by Fig. A1, the simulation indicates a marked improvement. Moreover, the effectiveness of simulation are influenced significantly by both N_k and R . While the period of time for which $-\ln L$ can be evaluated rigorously is enlarged by increasing N_k , the accuracy of computation is enhanced by increasing R . The error analysis will be presented in the next section.

B. Model II: the Singel-excitation dynamics in AAH model

Another exactly solvable situation is the open dynamics in the single-excitation subspace. For concreteness, we explore the single-excitation dynamics in the Aubry-André-Harper model (AAH) coupled to an Ohmic environment. The AAH model has recently been discussed intensively since the localization-delocalization transition can be observed in this model [21]. In this place, we examine the open dynamics by complex discretization approximation, as well as the exact numerics and the analytical evaluation as comparison.

The Hamiltonian of AAH model is written as [22]

$$H_s = J \sum_{n=1}^{N_s} (c_n^\dagger c_{n+1} + c_{n+1}^\dagger c_n) + \Delta \sum_{n=1}^{N_s} \cos(2\pi\beta n + \phi) c_n^\dagger c_n, \quad (35)$$

where J denotes the hopping strength, and Δ characterizes the strength of the onsite potential. c_n (c_n^\dagger) denotes the annihilation (creation) operator of excitations on the n -th chain point. $J \equiv 1$ is assumed for brevity. To avoid the effect of boundary, $c_{N_s+1} = c_1$ is imposed in the following calculation. It was well known that the critical point $\Delta = 2$ can separate the extended phase ($\Delta < 2$) from the localized phase ($\Delta > 2$) in the model. The recent studies showed that the localized phase would be destroyed because of the coupling to environment [23].

In the single-excitation subspace, the state of system can be formulated as

$$|\psi(t)\rangle = \left(\sum_{n=1}^{N_s} a_n(t) |1\rangle_n \right) |0\rangle^{\otimes k} + |0\rangle^{\otimes N_s} \left(\sum_k b_k(t) |1\rangle_k \right), \quad (36)$$

where $|1\rangle_n = c_n^\dagger |0\rangle$, $|0\rangle$ is the vacuum state of environment and $|1\rangle_k = b_k^\dagger |0\rangle$. Substituting Eq. (36) into

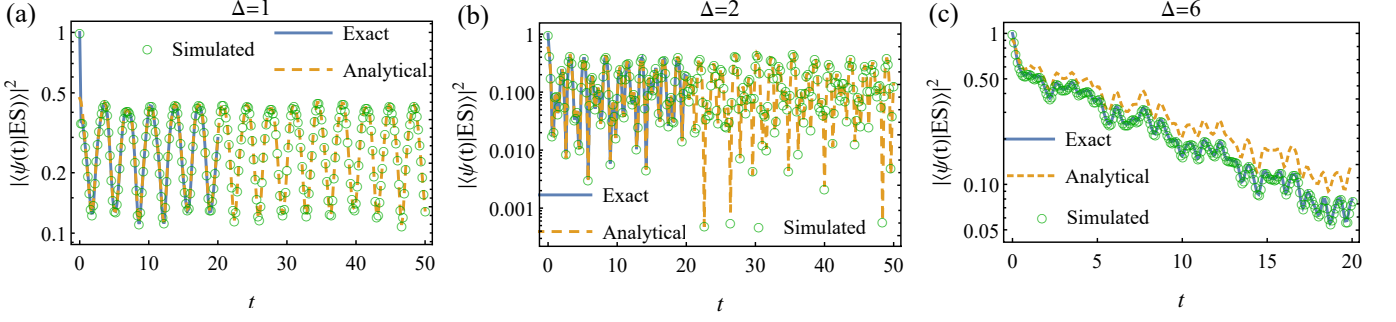


Figure 3. (Color online) The plot of $|\langle\psi(t)|ES\rangle|^2$ for $\Delta = 1, 2$ and 6 . To demonstrate the effectiveness of the CDA simulation (green empty circle), both the exact numerics (solid-blue line) and the analytical approach (dashed-orange line) are presented at the same time. For CDA simulation, $N_k = 2000$ and $R = 4.72$ are chosen, based on the error analysis shown in the next section. For all plots, we have chosen $N_s = 8, \beta = (\sqrt{5} - 1)/2, \phi = \pi$ and $\eta = 0.1, \omega_c = 10$. Especially, whereas the CDA simulation for $\Delta = 1, 2$ is attained by Eq. (30), we adopt Eq. (29) for $\Delta = 6$ to find the compliance with the exact numerics. The evolution time t is in units of $1/J$.

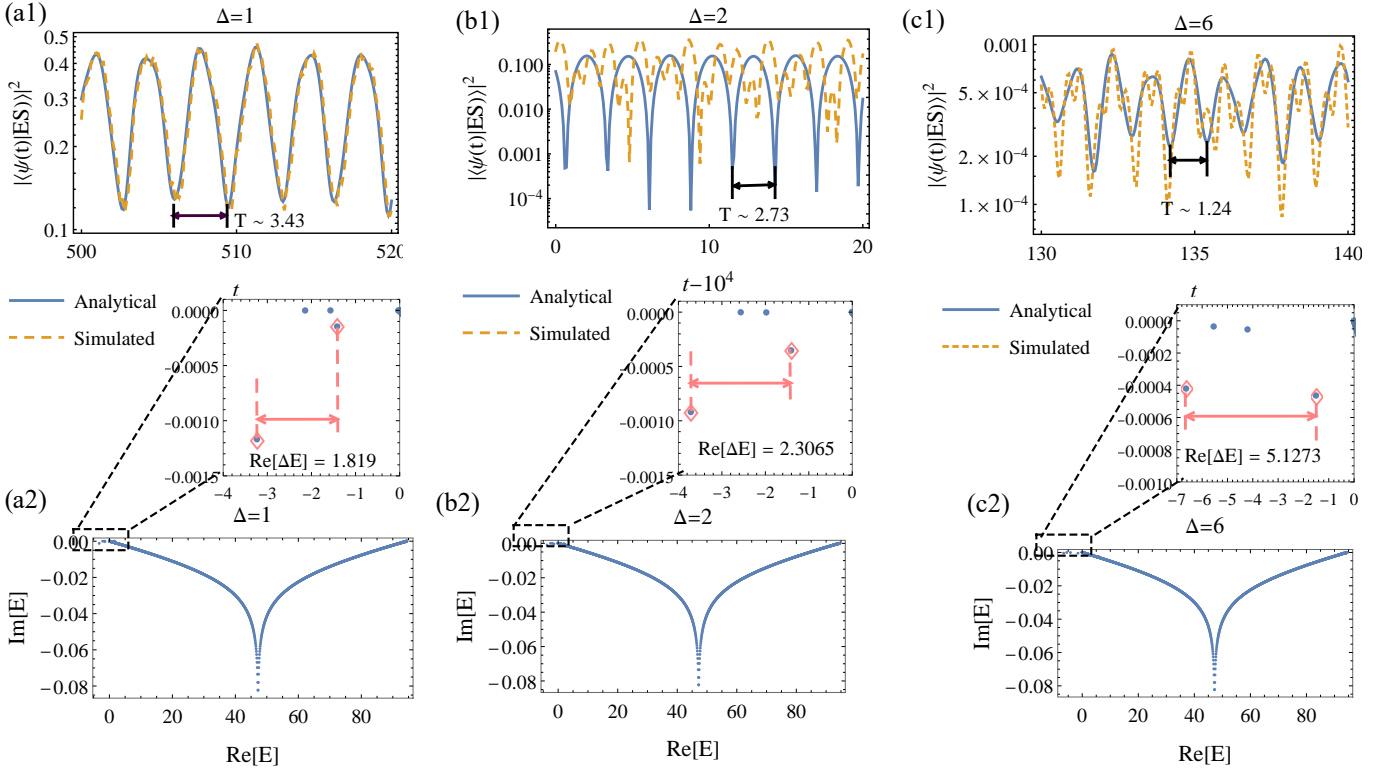


Figure 4. (Color online) (a1), (b1), (c1): The long term behavior for $|\langle\psi(t)|ES\rangle|^2$ when $\Delta = 1, 2$ and 6 . The evaluation of CDA simulation is shown by the dashed-orange line, while the analytical approach is shown by the solid-blue line. The value of T denotes the average period of oscillation of SP. The simulation of SP is implemented by Eq. (30) for $\Delta = 1, 2$, while it is done by Eq. (29) for $\Delta = 6$. Evolution time t is in units of $1/J$ (a2), (b2), (c2): The complex eigenvalue E (in units of J) of H_{eff} is obtained by solving the equation $H_{\text{eff}}|n\rangle_R = E_n|n\rangle_R$. The value of $\text{Re}[\Delta E]$ gives the difference between the two discrete energy levels, which are relevant to the observed oscillation illustrated in (a1), (b1), (c1). The other parameters are the same as in Fig. 3.

Schrödinger equation and eliminating $b_k(t)$, one gets

$$\begin{aligned} i \frac{\partial}{\partial t} a_n(t) &= [a_{n+1}(t) + a_{n-1}(t)] + \Delta \cos(2\pi\beta n + \phi) a_n(t) \\ &- i \sum_{n=1}^{N_s} \int_0^t d\tau a_n(\tau) \int_0^\infty d\omega J(\omega) e^{-i\omega(t-\tau)}, \end{aligned} \quad (37)$$

where i denotes the square root of -1 . Eq. (37) can be solved exactly by numerical iteration. However, due to the integrals involving time t , the iteration becomes so exhaustive for a long-time evolution. So, the exact numerics is restricted to the evolution for $t \leq 20$.

By Laplace transformation, Eq. (37) can be transformed into

$$i [pA_n(p) - a_n(0)] = \Delta \cos(2\pi\beta n + \phi) A_n(p) + A_{n+1}(p) + A_{n-1}(p) - \sum_m A_m(p) \int_0^\infty d\omega \frac{J(\omega)}{\omega - ip} \quad (38)$$

where $A_n(p) = \int_0^\infty dt a_n(t) e^{-pt}$. In principle, $A_n(p)$ can be decided by solving the system of equation above only if the integral can be evaluated. Thus, $a(t)$ can be determined by inverse Laplace transformation. In Appendix II, two distinct types of solutions for Eq. (38) has been determined. Thus, the analytical expression for $a_n(t)$ can be obtained, which provides the proper description for the mediated and long-term behavior of the system.

To demonstrate the effectiveness of CDA simulation, we simulate the single-excitation open dynamics of AAH model by calculating the survival probability (SP) $|\langle \psi(t) | ES \rangle|^2$, which depicts the preservation of quantum information against dissipation. The initial state $|ES\rangle$ represents the highest excited energy level in the AAH model, which is considered fragile in the presence of the dissipation due to its positive energy. The survival probability is plotted for $\Delta = 1, 2$ and 6 in Figs. 3, for which the AAH model can display the extended, critical and localized properties respectively. Additionally, the analytical and exact numerical evaluation are also provided to validate the simulation. The results show that the CDA simulation aligns perfectly with the analytical and exact numerical approaches.

There are some observations about the performance of simulation sketched in Figs. 3. First, as illustrated in the following section, the choice of $R = 4.72$ for $N_k = 2000$ is optimal. For this choice, the simulation is highly effective and reasonably accurate. Secondly, to simulate the stable oscillation illustrated in Fig. 3(a), the state $|\psi(t)\rangle$ is computed using Eq. (30), where the real part of E is utilized to establish the stability of dynamics. The efficacy of this choice is approved by the excellent agreement between the CDA simulation and the analytical approach, as illustrated by Fig. A5 (a1) in Appendix III. Furthermore, the agreement can persist even after a long term evolution, sketched by Fig. 4 (a1). This indicate that Eq. (30) offers a suitable description for the stability of the system.

When $\Delta = 2$, the behavior of SP is different, showing a stretched behavior, as illustrated by Fig. A4(b) in Appendix III. This behavior may be attributed to the critical property in the system. While Eq. (30) can simulate perfectly the evolution of SP for a short term as shown in Fig. 3(b), it fails to predict the long term behavior of SP, as shown in Fig. 4 (b1). Additionally, our explicit calculation reveals that using Eq. (30) does not significantly outperform using (29), as illustrated by Fig. A5 (b1) and (b2) in Appendix III.

For $\Delta = 6$, it has been observed that using Eq. (29) in the simulation is more effective than using Eq. (30). This is likely due to the exponential decaying of SP ob-

served in Fig. 3(c), which can be captured accurately by the negative imaginary part in the E . While the analytical evaluation for the short term evolutions becomes less accurate in this case, the exact numerics is employed up to $t = 20$. As shown in Fig. 3(c), the CDA simulation closely matches the numerical results. However, for a larger value of t , the computation becomes more exhaustive. The long term behavior of SP can be understood by the emergence of single-particle bound state. As shown in Fig. A4 (c), SP tends to be stable when $t > 100$. Interestingly, it is found that the CDA simulation can still present a qualitative understanding of the evolution of SP, as illustrated in Fig. 4 (c1). However, the simulation becomes divergent when $t > 160$.

The eigenvalue E obtained from the equation $H_{\text{eff}}|n\rangle_R = E_n|n\rangle_R$, is studied to understand the evolution of SP, as shown in Figs. 4. It is clear that there are multiple discrete energy levels present in the region $E < 0$, as shown in the panels (a2), (b2) and (c2) of Figs. 4. These energy levels seem to correspond to the single particle bound states, as their real parts closed match the energy of the bound state depicted in Fig. A3(a1)-(a3). This correspondence is further supported by determining the angular frequency for the stability of SP, which is entirely influenced by the single-particle bound states. In Figs. 4 (a2), (b2) and (c2), the calculated angular frequency is very similar to the energy difference between two energy levels in the $E < 0$ region.

Conclusively, the CDA method can provides the excellent simulation for the dynamics of AAH model. However, it is necessary to use different evolutions, such as Eq. (29) or Eq. (30), in order to effectively capture the unique dynamics of system. This may be due to the different physical characteristics associated with the stable oscillation, stretched dynamics and exponential decaying. The recent study has revealed that the open quantum system can undergo the dissipative phase transition, leading to the intrinsic changes in the system's dissipative dynamics [24]. The presence of three types of dissipation could be considered as a reflection of dissipative phase transition. Therefore, it is not surprising that using only one method cannot capture all three distinct dynamics of system.

V. ERROR ANALYSIS

To quantify the precision of the simulation, the section elaborates on the relative error in computation, which defined respectively as

$$\text{Error} = \frac{\text{Simulated} - \text{Exact}}{\text{Simulated} + \text{Exact}}, \quad (39)$$

$$\text{Error}' = \frac{\text{Simulated} - \text{Analytical}}{\text{Simulated} + \text{Analytical}}, \quad (40)$$

where ‘‘Simulated’’, ‘‘Analytical’’ and ‘‘Exact’’ denote the evaluation of SP respectively by CDA, analytical and exact numerical method.

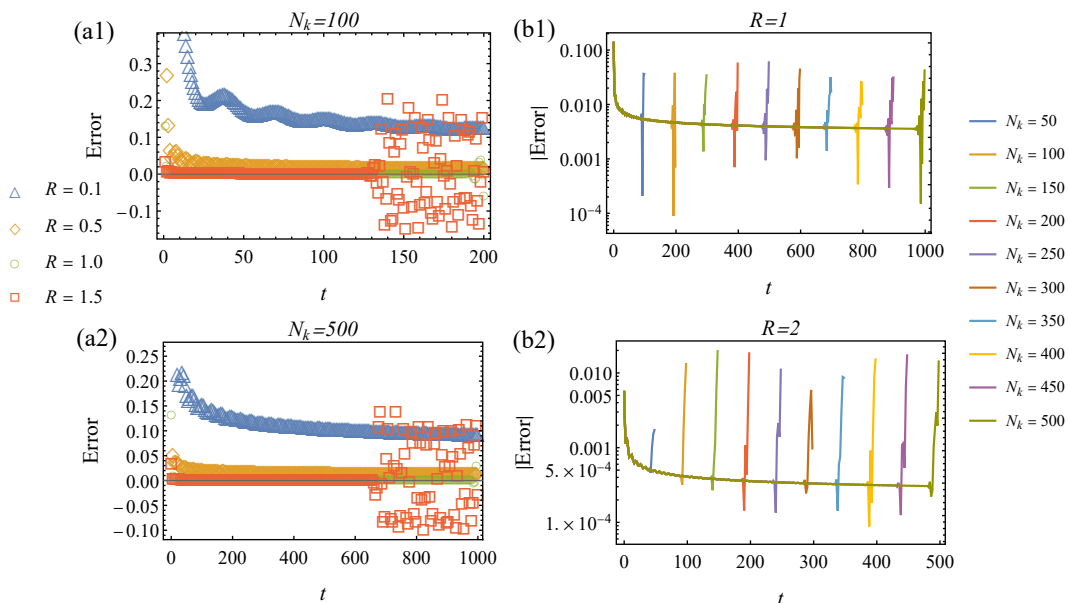


Figure 5. (Color online) The computational error defined by Eq. (39) for the evaluation of $-\ln L$ by CDA is plotted in panels (a1) and (a2) for different R . In panels (b1) and (b2), the modulus of the Error is plotted in logarithm for different values of N_k . All plots use the same parameters as those in Fig. 2. The evolution time t is in units of $1/\omega_c$.

A. Model I: the Dephasing model

Since the exact expression for L is known, the error defined by Eq. (39) is discussed explicitly in this case. The Error shows strong relevance to the values of R and N_k , as illustrated in Figs. 5. For a fixed N_k , increasing R leads to a significant reduction in the Error, as shown in panels (a1) and (a2). However, it is observed that the Error can start to fluctuate significantly after a certain time period t_p , which is obviously influenced by the value N_k . This time period, denoted as t_p , can be compressed when R is increased. Conversely, when R is kept constant, increasing N_k can significantly prolong t_p , although the error does not display a noticeable reduction as shown by panels (b1) and (b2).

In summary, the value R decides the accuracy of evaluation, while N_k is responsible for the efficiency of computation. A simple relationship of N_k , R and t_p can be established by analyzing the data, i.e.

$$Rt_p \simeq 2N_k, \quad (41)$$

which demonstrates clearly the combined influence of R and N_k on the evaluation of L .

B. Model II: the Single-excitation dynamics in AAH model

The error analysis becomes complicated due to the lack of the exact expression for SP in this model. To address this, we conducted a detailed investigation of the Error defined by Eq. (40) for $\Delta = 1$ in Figs. 6. This choice was

made because the analytical approach in this scenario can accurately characterize both the short term and long term behavior of SP, leading to clear conclusion. The simulation of SP is carried out using Eq. (30) in the plots, with a focus on the region where the modulus of Error' is less than 0.01. In Figs. 6, the boundary of this region is highlighted by the dashed white line. It is evident that the size of this region displays non-monotonic variance with the increase of R . Especially, after a enlargement for a relatively small R , this region becomes compressed when R exceeds a special value, termed as R_p . However, the value of Error' can be significantly reduced when R is greater than R_p . In Fig. 7, an exemplification is present for $N_k = 2000$, for which $R_p = 4.72$ can be decided by checking the evolution of Error'. It is obvious that the Error' displays a significant reduction when R approaches to 5 from below. However, the reduction can happen only in a finite evolution time when R is less than 5, and this effective evolution time is compressed with the further increasing of R . This finding means that one have to choose properly the value of R to attain the required precision. Obviously, R_p is significantly relevant to the value of N_k . The logarithmic fit to R_p is presented as a function of N_k in Fig. 8 (a).

Remarkably, a special time t_p related to R_p can be determined by analyzing Fig. 6. From Fig. 6, It is clear that the intersection of two dashed white line determines the maximum duration of evolution, when the modulus of Error' is not exceed 0.01. Similarly to the approach used in previous subsection, this time is also referred to as t_p , and signifies the duration during which the simulation remains effective. The relationship of t_p with N_k is shown in Fig. 8 (b), showing that t_p increases almost linearly

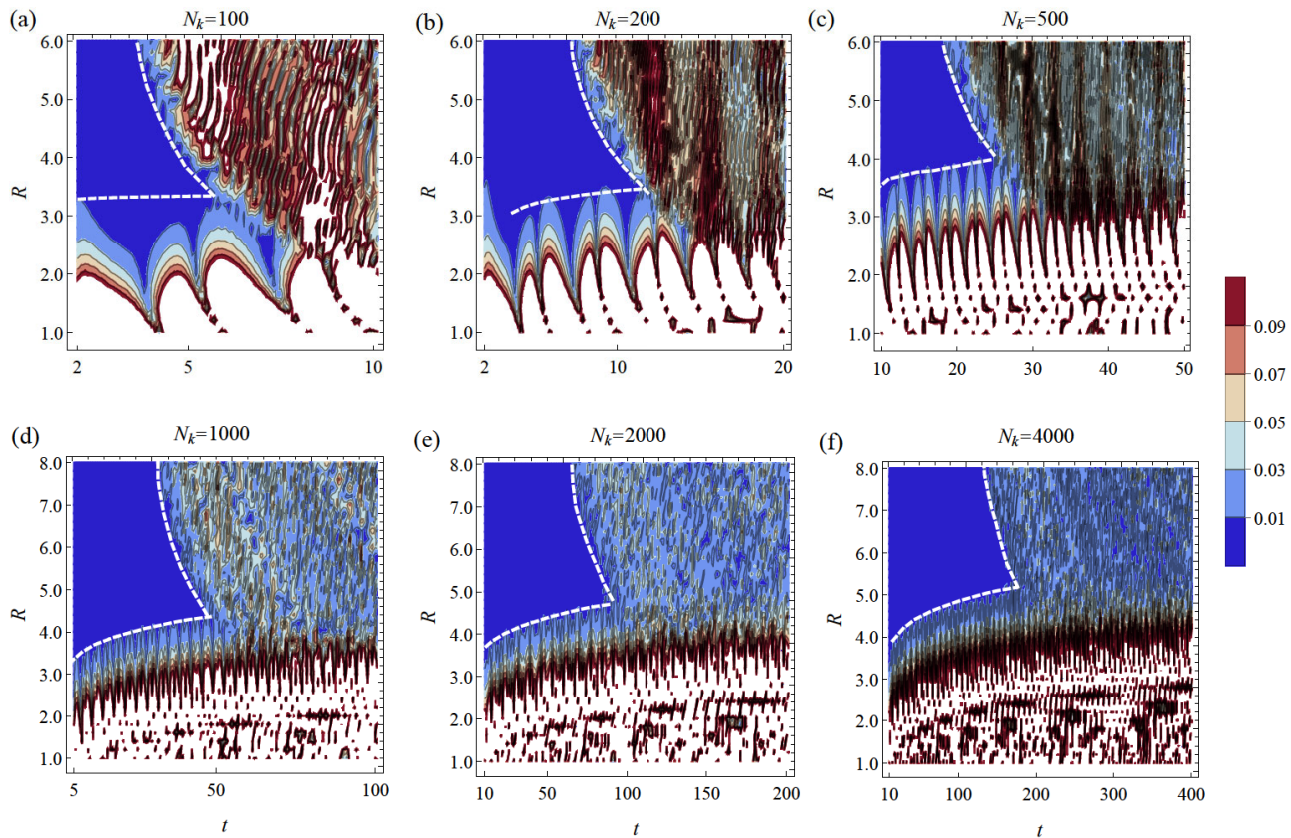


Figure 6. (Color online) The contour plot for the modulus of Error' defined by Eq. (40) when $\Delta = 1$ versus R and N_k . The other parameters are chosen as the same in Fig. 3. The dashed white line characterizes the boundary of the region, where the Error' is less than 0.01. For the plots, the simulation of SP is reached by Eq. 30. The evolution time t is in units of $1/J$.

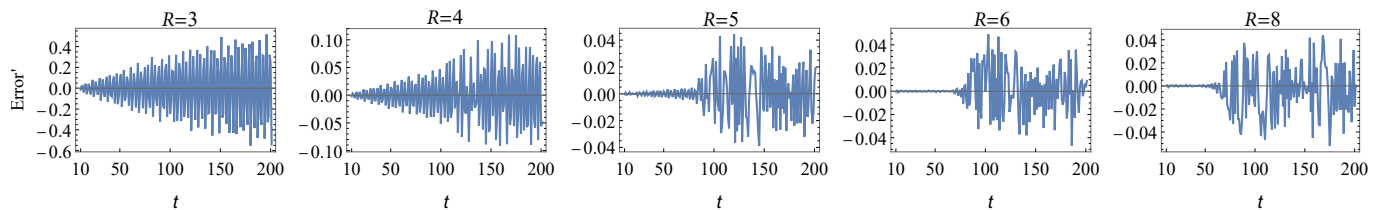


Figure 7. (Color online) The listed plot for the Error' when $\Delta = 1$ and $N_k = 2000$ versus selected values of R . All plots are done under the same setting as in Fig. 6. The evolution time t is in units of $1/J$.

with N_k .

It is important to note that both R_p and t_p are closely related to the desired threshold of error. A lower Error' leads to a smaller t_p and a larger R_p for a given N_k . Therefore, a balance must be struck between computational precision and the effective simulation time. Additionally, the study of $\Delta = 2$ and $\Delta = 6$ shows similar trends to $\Delta = 1$, as seen in the error analysis in the Appendix IV. However, drawing definitive conclusions in these cases is challenging due to the limited alignment between simulation results and analytical or exact numerical methods.

VI. CONCLUSION

This paper introduces a general approach for approximating the environment in continuum using gauss quadratures in the complex plane, which is termed as the complex discretization approximation. By this approach, an effective total Hamiltonian can be founded generally, which is nonHermitian and demonstrates complex energy mode with negative imaginary part. The method is then applied to simulate the open dynamics in two exactly solvable models, the dephasing model and single-excitation open dynamics in the AAH model. Compared to the real counterpart, the method can not only offer a significant advantage in compressing the recurrence in

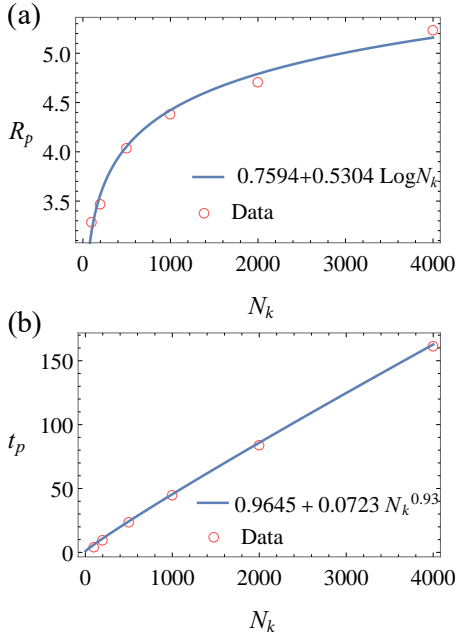


Figure 8. (Color online)(a) The logarithmic fit to R_p as a function of N_k . (b) The power fit to t_p as a function of N_k

dynamics because of the occurrence of complex energy modes, but also provides the microscopic description for the open dynamics of system through the effective Hamiltonian. Moreover, the error analysis reveals a simple relationship between the parameters in computation and the effectiveness of calculation. This means that one can manipulate the simulation in a controllable manner.

Finally, it should be stressed that the complex discretization approximation is fundamentally different from the method of pseudomode [26]. In the latter, the environment is discretized based on the complex poles of the spectral function $J(x)$, resulting in an enlarged open system with discrete modes. The dynamics of this system is captured by the Markovian Lindblad master equation. However, in the current method, the spectral function must be continuous in the lower half complex plane, and there is no need for the introduction of additional Markovian processes. The effective Hamiltonian obtained through this method can accurately describe the open dynamics of the system.

ACKNOWLEDGEMENTS

H.T.C. acknowledges the support of Natural Science Foundation of Shandong Province under Grant No. ZR2021MA036. Y. A. Y. acknowledges the support of National Natural Science Foundation of China (NSFC) under Grant No. 21973036. M.Q. acknowledges the support of NSFC under Grant No. 11805092 and Natural Science Foundation of Shandong Province under Grant No. ZR2018PA012. X.X.Y. acknowledges the support of NSFC under Grant No. 12175033 and National Key

R&D Program of China (No. 2021YFE0193500).

Appendix I. GAUSS QUADRATURES AND THE MAPPING TO CHAIN HAMILTONIAN

This appendix provides a succinct overview of the Gauss quadratures (GQ) and the process of converting the continuum setting into the chain form. The presentation follows mainly the references [14] and [18].

Gauss quadratures GQ is introduced to improve the numerical integration. Different from the equally spaced abscissas in the Newton-Cotes formula, GQ allows the freedom to choose not only the weight coefficients, but also the location of the abscissas at which the function is to be evaluated. It is crucial for GQ to construct orthogonal polynomials. For this purpose, one first defines the inner product for any polynomials $f(x), g(x)$

$$\langle f, g \rangle = \int_a^b dx w(x) f(x) g(x), \quad (\text{A1})$$

in which $w(x) \geq 0$ is the weight function defined on interval $x \in [a, b]$. Thus the polynomial $p_n(x) = x^n + \sum_{i=0}^{n-1} A_i x^i$ of degree n is orthogonal to $p_m(x)$ if it satisfies the relation

$$\langle p_m, p_n \rangle = \int_a^b dx w(x) p_m(x) p_n(x) = 0 (m \neq n). \quad (\text{A2})$$

With the assumption $p_0(x) = 1$ and $p_{-1}(x) = 0$, the recurrence relation can be deduce by Eq. (A2),

$$p_{n+1}(x) = (x - \alpha_n) p_n(x) - \beta_n p_{n-1}(x), \quad (\text{A3})$$

in which

$$\alpha_n = \frac{\langle x p_n, p_n \rangle}{\langle p_n, p_n \rangle}, \beta_n = \frac{\langle p_n, p_n \rangle}{\langle p_{n-1}, p_{n-1} \rangle}. \quad (\text{A4})$$

The proof can be found in Ref. [14] or [18].

The determination of the zero points of $p_n(x)$, denoted as $x_i (i = 1, 2, \dots, n)$, are crucial for the numerical integration. In order to find x_i , it is convenient to introduce orthonormalized polynomials $\pi_n(x) = p_n(x) / \sqrt{\langle p_n, p_n \rangle}$. Thus one has the orthonormality relation

$$\langle \pi_m, \pi_n \rangle = \int_a^b dx w(x) \pi_m(x) \pi_n(x) = \delta_{m,n}. \quad (\text{A5})$$

The recurrence relation becomes

$$\sqrt{\beta_{n+1}} \pi_{n+1}(x) = (x - \alpha_n) \pi_n(x) - \sqrt{\beta_n} \pi_{n-1}(x). \quad (\text{A6})$$

Alternatively, Eq. (A6) can be rewritten in a matrix form

$$x \begin{pmatrix} \pi_0 \\ \pi_1 \\ \vdots \\ \pi_{n-1} \end{pmatrix} = M_r \begin{pmatrix} \pi_0 \\ \pi_1 \\ \vdots \\ \pi_{n-1} \end{pmatrix} + \sqrt{\beta_n} \begin{pmatrix} 0 \\ 0 \\ \vdots \\ \pi_n \end{pmatrix};$$

$$M_r = \begin{pmatrix} \alpha_0 & \sqrt{\beta_1} & 0 & \cdots \\ \sqrt{\beta_1} & \alpha_1 & \ddots & 0 \\ 0 & \ddots & \ddots & \sqrt{\beta_{n-1}} \\ 0 & \cdots & \sqrt{\beta_{n-1}} & \alpha_{n-1} \end{pmatrix}, \quad (\text{A7})$$

in which π_n implies $\pi_n(x)$. Thus, x_i corresponds to the eigenvalue of symmetric matrix M_r . The corresponding orthonormalized eigenvector $|x_i\rangle$ can be determined by normalizing $(\pi_0(x_i), \pi_1(x_i), \dots, \pi_{n-1}(x_i))^T$.

The weight w_i for x_i can be decided by the Christoffel-Darboux identity. It has been proved that w_i satisfies the relation [18]

$$w_i \sum_{k=0}^{n-1} [\pi_k(x_i)]^2 = 1 \quad (i = 1, 2, \dots, n). \quad (\text{A8})$$

In practice, it is more convenient to determine w_i by the equivalence

$$\sqrt{w_i} (\pi_0(x_i), \pi_1(x_i), \dots, \pi_{n-1}(x_i))^T \Rightarrow |x_i\rangle. \quad (\text{A9})$$

By $|x_i\rangle = (q_0^{(i)}, q_1^{(i)}, \dots, q_{n-1}^{(i)})^T$, which can be obtained directly by numerics, one gets

$$w_i = \left[\frac{q_0^{(i)}}{\pi_0(x_i)} \right]^2 = [q_0^{(i)}]^2 \int_a^b dx w(x). \quad (\text{A10})$$

In summary, the following theorem can be found [18],

Theorem 1 *Let $w(x)$ be a weight function on the interval $[a, b]$. Then the polynomials $\pi_n(x)$ can present real zero points x_i and corresponding weight $w_i (i = 1, 2, \dots, n)$, which show the properties (i) $a < x_i < b (\forall i)$; (ii) $w_i > 0 (\forall i)$; (iii) The equivalence*

$$\int_a^b dx w(x) f(x) = \sum_{i=0}^{n-1} w_i f(x_i) \quad (\text{A11})$$

is exactly true for polynomial $f(x)$ of degree $\leq (2n - 1)$.

Some comments should be made in this place. First, the choice of $w(x)$ is important, as it determines entirely the polynomials $\pi_n(x)$. Generally, there is no mathematical restriction on the choice of $w(x)$. However, it is ideal to relate $w(x)$ with the physical quantity. For instance it can be constructed, based on the spectral function $J(x)$, as shown in the following illustrations. Secondly, x_i displays different contribution to the evaluation, weighted by w_i . In regard to the open quantum system, it implies

that certain modes of environment would dominate the open dynamics of system. Finally, in the event that $f(x)$ is a series or the upper bound approach infinity, the integration can solely be deemed precise only if n approaches infinity. Thus, the degree of accuracy in the evaluation is contingent upon the value of n .

Mapping to Chain form- In order to discretize the continuum in environment, one can introduce the transformation [14]

$$d_n = \int_a^b dx \sqrt{w(x)} \pi_n(x) b_x. \quad (\text{A12})$$

and the inverse

$$b_x = \sqrt{w(x)} \sum_{n=0}^{N_k-1} \pi_n(x) d_n, \quad (\text{A13})$$

in which N_k denotes the highest degree of polynomial used in evaluation. It can be proved directly

$$\begin{aligned} [d_n, d_m^\dagger] &= \iint dx dx' \sqrt{w(x)w(x')} \pi_n(x) \pi_m(x') [b_x, b_{x'}^\dagger] \\ &= \int_a^b dx w(x) \pi_n(x) \pi_m(x) = \delta_{n,m}, \end{aligned} \quad (\text{A14})$$

where $[b_x, b_{x'}^\dagger] = \delta(x - x')$ is applied. Substituting Eq. (A13) into H_b , one gets

$$H_b = \omega_c \sum_{m,n} d_m^\dagger d_n \int_a^b dx w(x) \pi_m(x) x \pi_n(x), \quad (\text{A15})$$

in which $h(x) = \omega_c x$ is used. Replacing $x \pi_n(x)$ according to Eq. (A6), one gets

$$\begin{aligned} H_b &= \omega_c \sum_{m,n} \left(\alpha_n \delta_{m,n} + \sqrt{\beta_{n+1}} \delta_{m,n+1} + \sqrt{\beta_n} \delta_{m,n-1} \right) d_m^\dagger d_n \\ &= \omega_c (\dots, d_m^\dagger, \dots) M_r \begin{pmatrix} \vdots \\ d_n \\ \vdots \end{pmatrix}, \end{aligned} \quad (\text{A16})$$

where M_r is given by Eq. (A7). Evidently, H_b is transformed into a chain form with the nearest neighbor hopping.

Accordingly, H_{int} can be rewritten as

$$H_{\text{int}} = \sum_n \sum_{i=1}^{N_k} \int_a^b dx \sqrt{w(x)} \pi_i(x) [g(x) c_n^\dagger d_i + g^*(x) d_i^\dagger c_n] \quad (\text{A17})$$

Assuming that $g(x)$ is real and setting $w(x) = g^2(x)$, one thus obtain

$$\begin{aligned} H_{\text{int}} &= \sum_n \sum_{i=1}^{N_k} \int_a^b dx w(x) \pi_i(x) [c_n^\dagger d_i + d_i^\dagger c_n] \\ &= \sqrt{\int_a^b dx w(x)} \sum_n (c_n^\dagger d_0 + d_0^\dagger c_n), \end{aligned} \quad (\text{A18})$$

in which the orthonormality relation Eq. (A5) is applied for the second equality. It is evident that Eq. (A18) features the coupling of system to the end of chain, depicted by Eq. (A16).

Eqs. (A16) and (A18) are subject to certain comments. First, the transformation Eq. (A13) is unitary only when $N_k \rightarrow \infty$. Only in this situation, Eqs. (A16) and (A18) can be considered equivalent exactly to H_b and H_{int} in Eq. (1). Therefore, a large N_k as possible is necessary to accurately simulate the open dynamics of system. However, it makes the computation very exhaustive. Secondly, a reasonable choice of $w(x)$ can facilitate numerical simulation. Evidently, the choice of $w(x) = g^2(x)$ gives the straightforward physical interpretation for H_{int} . Finally, by diagonalizing Eq. (A16), one gets

$$H_b = \omega_c \sum_{i=1}^{N_k} x_i \tilde{d}_i^\dagger \tilde{d}_i \quad (\text{A19})$$

$$H_{\text{int}} = \sum_n \sum_{i=1}^{N_k} \sqrt{w_i} \left(c_n^\dagger \tilde{d}_i + \tilde{d}_i^\dagger c_n \right) \quad (\text{A20})$$

where $\tilde{d}_i^\dagger, \tilde{d}_i$ denote the creation and annihilation operator relevant to the energy level $\omega_c x_i$. It is obvious that x_i characterizes the discrete energy mode in environment. As a consequence, the discretization approximation for environment is reduced to find the zero points of polynomial $\pi_{N_k}(x)$.

Illustration- In order to highlight the advantage of CDA developed in the maintext, the open dynamics in two exactly solvable models are reexamined in this real place.

The dephasing model

It is convenient to choose $w(x) = g^2(x) = x e^{-x}$. Replacing H_b and H_{int} by Eqs. (A19) and (A20), one can obtain finally

$$-\ln L \simeq \sum_{i=0}^{N_k-1} w_i \frac{1 - \cos x_i t}{x_i^2}. \quad (\text{A21})$$

A comparison for Eq. (A21) with the exact result Eq. (33) is depicted in Fig. A1. It is evident that the recurrence due to a finite N_k can be developed rapidly after a finite time. Therefore, to obtain the long-term behavior of $-\ln L$, a large N_k is required, which however makes the computation expensive.

The single-excitation open dynamics in AAH model

We choose $w(x) = g^2(x) = \eta \omega_c^2 x^s e^{-x}$. Thus, H_b or H_{int} is transformed into Eqs. (A19) or (A20) respectively. The survival probability $|\langle \psi(t) | ES \rangle|^2$ is plotted in Fig. A2. The exact result of $|\langle \psi(t) | ES \rangle|^2$ is obtained

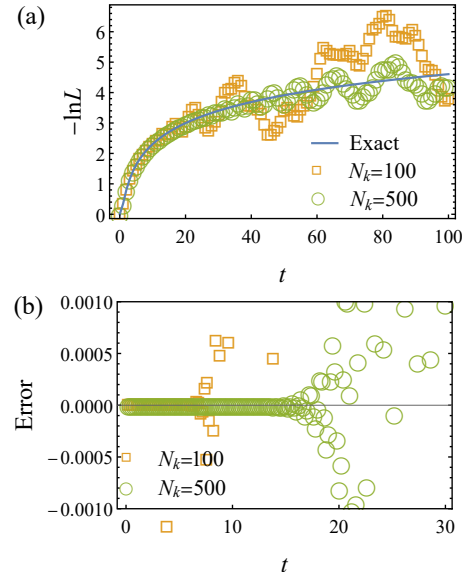


Figure A1. (Color online) A Comparative plotting of decoherence factor L . (a) The solid line depicts the exact results Eq. (33). The empty orange square and green circle plot the results obtained by discretization approximation in real space with the polynomial of degree $N_k = 100, 500$ respectively. (b) the computational error is demonstrated for different N_k . The evolution time t is in units of $1/\omega_c$.

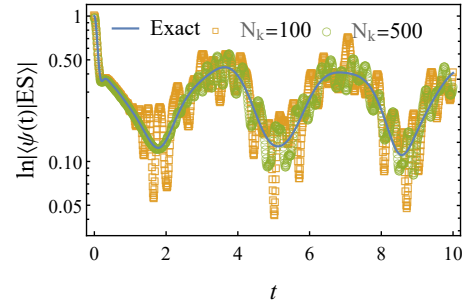


Figure A2. (Color online) A Comparative plotting of $|\langle \psi(t) | ES \rangle|^2$. The solid line depicts the results obtained by solving Eq. (37). The empty orange square and green circle plot the results obtained by discretization approximation with the polynomial of degree $N_k = 100, 500$ respectively. For this plot, we have chosen $N_s = 8, \beta = (\sqrt{5} - 1)/2, \phi = \pi, \Delta = 1$ and $\eta = 0.1, \omega_c = 10$. The evolution time t is in units of $1/J$.

by solving Eq.(36). Similar to the previous case, the recurrence becomes pronounced significantly after a short time period. This feature underscores the necessity to improve the discretization approximation to enable the efficient simulation of open dynamics of many-body systems.

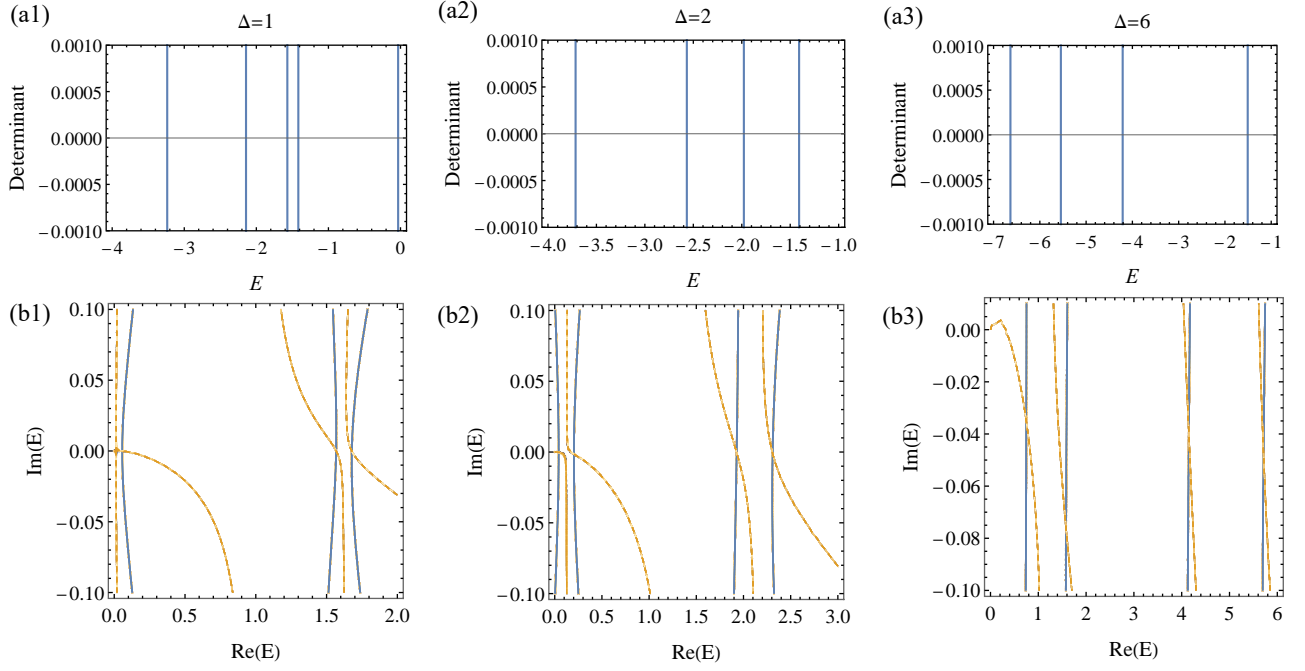


Figure A3. (Color online) (a1) - (a3): The plots for the determinate of coefficient matrix of Eq. (A24) when $E < 0$. (b1) - (b3): The determinate of coefficient matrix of Eq. (A24) is plotted by a contour of value zero for the complex E with positive real part. The solid line denotes the real part of the determinant, and the dashed line denotes the imaginary part. The intersection implies the existence of the decaying energy level. For all plots, we have chosen $N_s = 8, \beta = (\sqrt{5} - 1)/2, \phi = \pi$ and $\eta = 0.1, \omega_c = 10$. The E is in units of J

Appendix II. ANALYTICAL APPROACH TO THE SINGLE EXCITATION OPEN DYNAMICS IN AAH MODEL

This appendix provides the analytical approach to the single-excitation open dynamics of AAH model by solving Eq. (38). Mathematically, Eq. (38) represents the linear system of equation for the unknown $A_n(p)$ s. In principle, one can find all $A_n(p)$ by Cramer's rule, only if the integral $\int_0^\infty d\omega \frac{J(\omega)}{\omega - ip}$ is evaluated accurately. Then, $a(t)$ can be obtained analytically using inverse Laplace transformation. There are two specific scenarios, where the solution to Eq. (38) can analytically determined.

-*The single particle bound state*- When $ip = E$ with $E < 0$, the physical interpretation of E can be elucidated through inverse Laplace transformation, defined formally as

$$a_n(t) = \frac{1}{2\pi i} \int_{s-i\infty}^{s+i\infty} dp A_n(p) e^{pt}. \quad (\text{A22})$$

In analogy to the evolution operator in quantum mechanics, $A_n(p)$ can be viewed as the probability amplitude, with E representing the eigenvalue of the Hamiltonian. This relationship between E and the corresponding $A_n(p)$ defines the unitary evolution that governs the stable behavior in the open dynamics of the system.

Typically, the value of E is determined by solving the equation $H|\psi\rangle = E|\psi\rangle$. In the single-excitation subspace,

the total state $|\psi\rangle$ can be written formally as

$$|\psi\rangle = \left(\sum_{n=1}^{N_s} a_n |1\rangle_n \right) |0\rangle^{\otimes k} + |0\rangle^{\otimes N_s} \left(\sum_k b_k |1\rangle_k \right) \quad (\text{A23})$$

Eliminating the dependence on b_k , one gets

$$a_{n+1} + a_{n-1} + \Delta \cos(2\pi\beta n + \phi) a_n + \sum_{n=1}^N a_n \int_0^\infty d\omega \frac{J(\omega)}{E - \omega} = E a_n. \quad (\text{A24})$$

The solution to the above equation in the region $E < 0$ can be determined by setting the determinant of the coefficient matrix for variables $(a_1, a_2, \dots, a_{N_s})^T$ equal to zero. In Figs. A3(a1)-(a3), the determinant of coefficient matrix is plotted to identify the values of E . Evidently, the intersection of the determinant and the E -axis can be found at some isolated values of E . These discrete energy levels are denoted as the single particle bound state s [27]. Because of the finite energy gap from the continuum $\omega_k \in [0, \infty)$, the single particle bound state can display the robustness against the dissipation induced by the coupling to environment [28].

Once $p = -iE_k$ is given, the values of $(A_1(p), A_2(p), \dots, A_{N_s}(p))$ can be derived by solving Eq. (38). Since the coefficient matrix in Eq. (38) is identical to that in Eq. (A24), E_k represents a singular point in the expression for $A_n(p)$ ($n = 1, 2, \dots, N_s$),

which can be obtained by applying Cramer's rule to Eq. (38). This singularity allows for the straightforward evaluation of Eq. (A22) using the residual theorem, i.e.

$$a_n(t) \rightarrow \sum_k c_n(E_k) e^{-iE_k t}, \quad (\text{A25})$$

$$c_n(E_k) = \lim_{E \rightarrow E_k} A_n(p) (E - E_k).$$

-*The decaying state*- The integral $\int_0^\infty d\omega \frac{J(\omega)}{\omega - E}$ becomes divergent when $E > 0$. This problem can be resolved by adding an imaginary item in the denominator, such as $\omega \rightarrow \omega - i\epsilon$ with infinitesimal $\epsilon > 0$. Then by Sokhotski-Plemelj (SP) formula

$$\lim_{\epsilon \rightarrow 0} \frac{1}{x - x_0 - i\epsilon} = \text{P} \frac{1}{x - x_0} + i\pi\delta(x - x_0), \quad (\text{A26})$$

one can get

$$\lim_{\epsilon \rightarrow 0} \int_0^\infty d\omega \frac{J(\omega)}{\omega - E - i\epsilon} = \text{P} \int_0^\infty d\omega \frac{J(\omega)}{\omega - E} + i\frac{\pi}{2} J(E), \quad (\text{A27})$$

where P denotes the principle value. In this manner, the decaying energy level can be determined. The decaying energy level is complex and displays a negative imaginary part, which can characterize the dissipation in the system.

Assuming $E = x + iy$ with real x, y and $x > 0$, and substituting this expression into Eq. (A24), one can get the decaying energy level by setting the determinant of coefficient matrix equal to zero. In Fig. A3 (b1)-(b3), the real and imaginary parts of the determinate is plotted by a contour of zero value, in which the intersection of the solid and dashed line represents the occurrence of the decaying energy level. The explicit calculation shows that the decaying energy level closed to the axis $\text{Im}(E) = 0$ has negative imaginary part, which accurately describes the open dynamics in AAH model. The corresponding inverse Laplace transformation can be carried out in the same way as described in the previous part. However, it is noted that the intersection can also be found far away from the axis $\text{Im}(E) = 0$. The explicit calculation shows that these state would be unphysical since they can introduce the gain effect in the dynamics or result in a SP greater than unity. Unfortunately, we do not know currently how to preclude the unphysical intersection during the evaluation.

Conclusively, one can determine the open dynamics of AAH model analytically using

$$a_n(t) \simeq \sum_k c_n(E_k) e^{-iE_k t} + \sum_k c_n(x_k + iy_k) e^{-i(x_k + iy_k)t}, \quad (\text{A28})$$

The first summation in the equation above representing the contribution of the single particle bound state, depicts the long term behavior of the dynamics, while the second summation characterizes the intermediated term dynamics from the decaying states. As shown in Fig. 3, the calculation by this equation aligns well with the exact numerical evaluation and CDA simulation. However,

for a very small t , Eq. (A28) may not be accurate and the exact numerical evaluation is recommended in such case.

In Fig. A4, the long term evolution for $|\langle \psi(t) | ES \rangle|^2$ is evaluated by Eq. (A28). Evidently, three distinct types of dynamics can be observed: (a) stable oscillation, (b) stretched dynamics and (c) exponentially fast decaying. Especially for $\Delta = 2$, SP tends to be stable after a period of time $\sim 3.0 \times 10^3$. In contrast, SP becomes stable after a period of time ~ 10 or ~ 100 when $\Delta = 1$ or 6 respectively. This is what is meant by the term "stretched dynamics".

Appendix III. FURTHER DISCUSSION ABOUT THE USAGE OF EQ. (29) AND EQ. (30) TO SIMULATE THE EVOLUTION OF SP

In Fig. 3, we have employed either Eq. (29) or Eq. (30) to simulate the evolution of SP for different values of Δ . The choice is based on the observation presented in Figs. A5. In Figs. A5 (a1) and (a2), we check the Error' defined by Eq. (40) when $\Delta = 1$. While the Error' calculated using (29) could be reduced by increasing N_k , it is generally negative, as illustrated in Fig. A5 (a2). On the other hand, the Error' derived from Eq. (30) exhibits significant oscillation around the zero line, regardless of N_k as depicted in Fig. A5 (a1). This suggests that Eq. (30) can offer more stable evaluation of SP compared to Eq. (29). However, Fig. A5 (a1) indicate an increasing in the amplitude of oscillation with larger N_k . This feature is a result of the presence of R_p defined in section V, which increases with N_k and influences the effectiveness of CDA.

However, when $\Delta = 6$, the lack of reliable analytical approaches necessitates the study of the error defined by Eq. (39). As shown in Figs. A5, it is clear that the Error obtained from Eq. (29) (panel (c2)) is obviously smaller than that from Eq. (30) (panel (c1)). This indicates that Eq. (29) can accurately capture the decaying dynamics of system, while Eq. (30) may be more suitable for simulating the stable dynamics of system.

In the case where $\Delta = 2$, a particulate scenario arises. It is noted that the error defined by Eq. (40) exhibits weak sensitivity to the selection between Eq. (30) or Eq. (29), as depicted in Figs. A5 (b1) and (b2). This could be due to the stretched behavior of SP at this stage, which represents an intermediate phase between stable and decaying evolution. Consequently, both Eq. (30) and Eq. (29) are unable to accurately capture this unique dynamics.

Appendix IV. SUPPLEMENTAL DISCUSSION ABOUT THE ERROR ANALYSIS

This appendix presents a study on the computational error in the case of $\Delta = 2$ and 6. Fig. A6 shows a

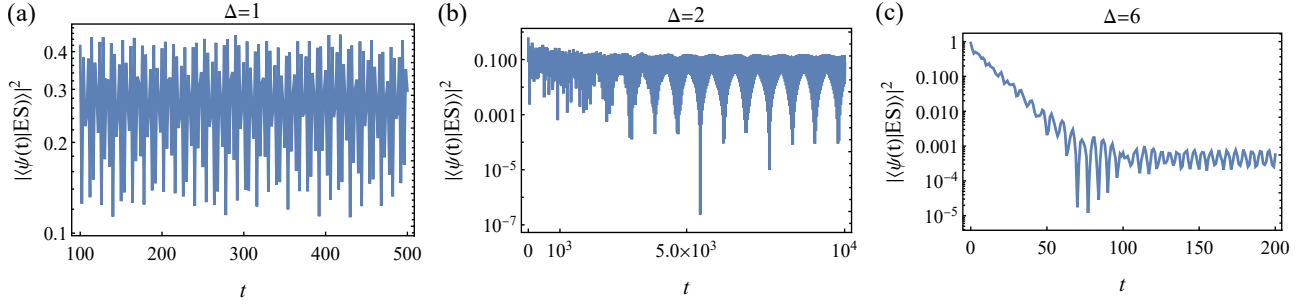


Figure A4. (Color online) The long term behavior for SP obtained by Eq. (A28). For all plots, we have chosen $N_s = 8$, $\beta = (\sqrt{5} - 1)/2$, $\phi = \pi$ and $\eta = 0.1$, $\omega_c = 10$. The evolution time t is in units of $1/J$

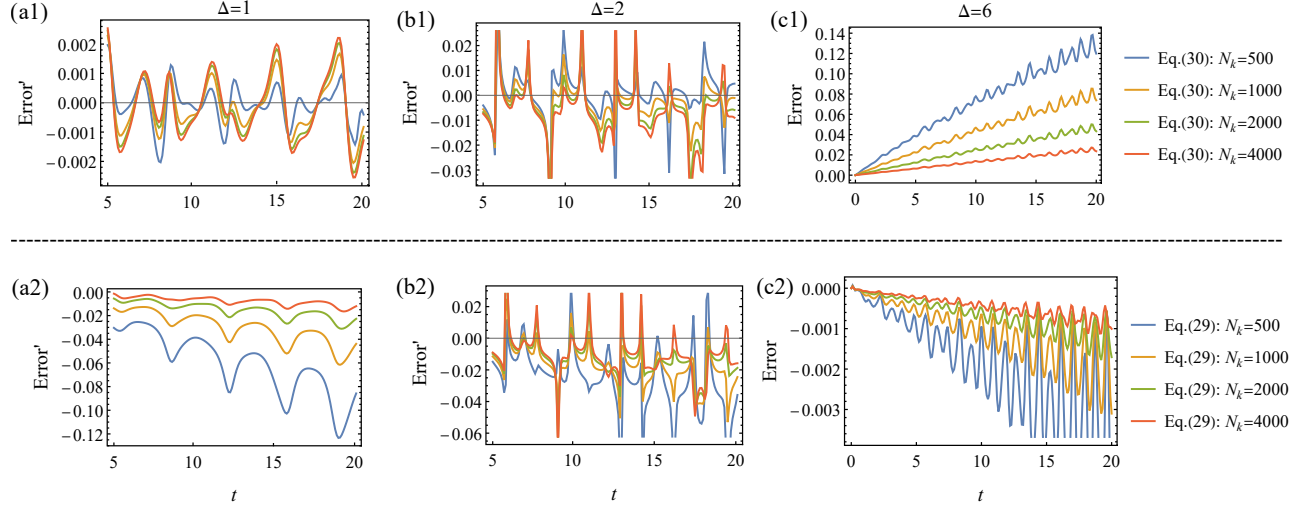


Figure A5. (Color online) The comparative plots for the computational error evaluated by Eq. (39) or Eq. (40) respectively. In panels (a1), (a2), (b1) and (b2), the error defined by Eq. (40) is evaluated for $\Delta = 1$ and 2 . While the error defined by Eq. (39) is evaluated only for $\Delta = 6$ in panels (c1) and (c2) because of the incomppliance of the analytical approach and exact numerics in this case. The evolution time t is in units of $1/J$

contour plot for the Error' when $\Delta = 2$. Although the similar feature as Fig. 6 can be noted, there are strong fluctuations, making it challenging to determine the value of R_p or t_p . This could be due to the stretched behavior of SP in this case, leading to less alignment between the simulation and analytical approach.

For $\Delta = 6$, the analytical approach is not unreliable for short term evolution. Therefore, the error analysis is

based on exact numerical results, which can be obtained only for a short term evolution. The simulation of SP can be done effectively by Eq. (29) in this case, as discussed in the Appendix III. Fig. A7 shows a contour plot of the Error for $N_k = 100, 200$. The value of R_p can be identified, which is close to that for $\Delta = 1$. For larger N_k , the value of t_p may exceed the attainability of the exact numerics.

- [1] H. P. Breuer, F. Petruccione, *The Theory of Open Quantum Systems*, Oxford University Press (2002).
- [2] I. M. Georgescu, S. Ashhab, Franco Nori, *Quantum Simulation*, Rev. Mod. Phys. **86**, 154 (2014); M. Gong, *et.al.*, *Quantum walks on a programmable two-dimensional 62-qubit superconducting processor*, Science, **372**, 948-952 (2021); Q. Zhu, *et.al.*, *Quantum computational advantage via 60-qubit 24-cycle random circuit sampling*, Science Bulletin, **67**(3), 240-245 (2022).
- [3] A. F. Kockum, A. Miranowicz, S. De Liberato, S. Savasta

- and F. Nori, *Ultrastrong coupling between light and matter*, Nat. Rev. Phys. **1**, 19-40 (2019); P. Forn-Diaz, L. Lamata, E. Rico, J. Kono, and E. Solano, *Ultrastrong coupling regimes of light-matter interaction*, Rev. Mod. Phys. **91**, 025005.
- [4] A. W. Chin, S. F. Huelga and M. B. Plenio, *Coherence and decoherence in biological systems: principles of noise-assisted transport and the origin of long-lived coherences*, Phil. R. Soc. A, **370**, 3638-3657 (2012); A. Ivanov, H. P. Breuer, Phys. Rev. A **92**, 032113 (2015); F. Caycedo-

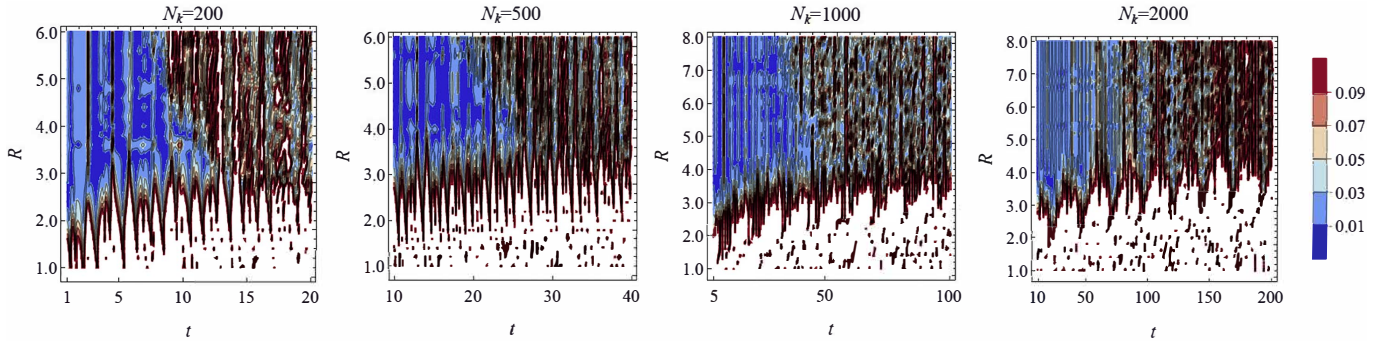


Figure A6. (Color online) The contour plot for the modulus of Error' defined by Eq. (40) when $\Delta = 2$ versus R and N_k . The other parameters are chosen as the same in Fig. 3. For all plots, the simulation of SP is reached by Eq. 30. The evolution time t is in units of $1/J$

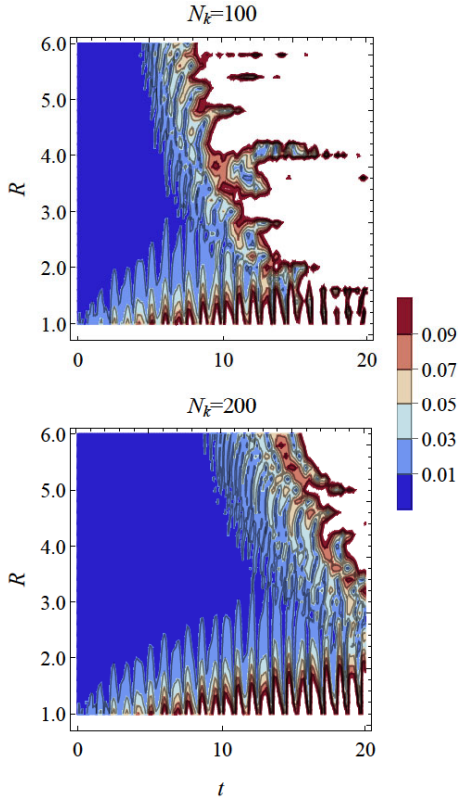


Figure A7. (Color online) The contour plot for the modulus of Error defined by Eq. (39) when $\Delta = 6$ versus R and N_k . The other parameters are chosen as the same in Fig. 3. Especially, the simulation of SP is reached by Eq. 29 in this case. The evolution time t is in units of $1/J$

Soler, A. Mattioni, J. Lim, T. Renger, S. F. Huelga, M. B. Plenio, *Exact simulation of pigment-protein complexes unveils vibronic renormalization of electronic parameters in ultrafast spectroscopy*, Nat. Commun. **13**, 2912 (2022).

- [5] F. Binder, L. A. Correa, C. Gogolin, J. Anders, and G. Adesso, *Thermodynamics in the Quantum regime*, Springer, Cham, Switzerland (2018); G. T. Landi and M. Paternostro, *Irreversible entropy production: From clas-*

sical to quantum, Rev. Mod. Phys. **93**, 035008 (2021).

- [6] E. Zerah-Harush and Y. Dubi, *Effect of disorder and interactions in environment assisted quantum transport*, Phys. Rev. Research, **2**, 023294 (2020); N. C. Cháves, F. Mattiotti, J. A. Méndez-Bermúdez, F. Borgonovi, and G. Luca Celardo, *Disorder-enhanced, and disorder-independent transport with long-range hopping: application to molecular chains in optical cavities*, Phys. Rev. Lett. **126**, 153201 (2021); D. Dwiputra, and F. P. Zen, *Environment-assisted quantum transport and mobility edges*, Phys. Rev. A **104**, 022205 (2021).
- [7] I. de Vega, D. Alonso, *Dynamics of non-Markovian open quantum systems*, Rev. Mod. Phys. **89**, 015001 (2017).
- [8] S. Nakajima, *On Quantum Theory of Transport Phenomena: Steady Diffusion*, Prog. Theor. Phys. **20**, 948 (1958); R. Zwanzig, *Ensemble Method in the Theory of Irreversibility*, J. chem. Phys. **33**, 1338 (1960).
- [9] F. Shibata, Y. Takahashi, and N. Hashitsume, *A generalized stochastic Liouville equation. NonMarkovian versus memoryless master equations*, J. Stat. Phys. **17**, 171 (1977); S. Chaturvedi and F. Shibata, *Time-convolutionless projection operator formalism for elimination of fast variables. Applications to Brownian motion*, Z. Phys. B **35**, 297 (1979); F. Shibata and T. Arimitsu, *Expansion Formulas in Nonequilibrium Statistical Mechanics*, J. Phys. Soc. Jpn. **49**, 891 (1980).
- [10] J. Cao, L. W. Ungar, and G. A. Voth, *A novel method for simulating quantum dissipative systems*. J. Chem. Phys. **104**, 4189 (1996); Y.-A. Yan, J.-S. Shao, *Stochastic description of quantum Brownian dynamics*, Front. Phys. **11**, 110309 (2016).
- [11] Y. Tanimura and R. Kubo, *Time Evolution of a Quantum System in Contact with a Nearly Gaussian-Markoffian Noise Bath*, J. Phys. Soc. Jpn. **58**, 101(1989); Y.-A. Yan, F. Yang, Y. Liu, and J.-S. Shao, *Hierarchical approach based on stochastic decoupling to dissipative systems*, Chem. Phys. Lett. **395**, 216-221 (2004).
- [12] N. Makri and D. E. Makarov, *Tensor propagator for iterative quantum time evolution of reduced density matrices. I. theory*, J. Chem. Phys. **102**, 4600 (1995); *ibid.*, *Tensor propagator for iterative quantum time evolution of reduced density matrices. II. Numerical methodology*, J. Chem. Phys. **102**, 4611 (1995).
- [13] R. Rosenbach, J. Cerrillo, S. F. Huelga, J. Cao, and M. B. Plenio, *Efficient simulation of non-Markovian system-*

- environment interaction, *New J. Phys.* **18**, 023035 (2016); A. Strathearn, P. Kirton, D. Kilda, J. Keeling, and B. W. Lovett, *Efficient non-Markovian quantum dynamics using time-evolving matrix product operators*, *Nat. Commun.* **9**, 3322 (2018);
- [14] A. W. Chin, Á. Rivas, S. F. Huelga, and M. B. Plenio, *Exact mapping between system-reservoir quantum models and semi-infinite discrete chains using orthogonal polynomials*, *J. Math. Phys.* **51**, 092109 (2010); M. P. Woods, R. Groux, A. W. Chin, S. F. Huelga, and M. B. Plenio, *Mappings of open quantum systems onto chain representations and Markovian embeddings*, *J. Math. Phys.* **55**, 032101 (2014).
- [15] R. Trivedi, D. Malz, and J. I. Cirac, *Convergence guarantees for discrete mode approximation to non-Markovian quantum baths*, *Phys. Rev. Lett.* **127**, 250404 (2021).
- [16] R. S. Burkey, C. D. Cantrell, *Discretization in the quasi-continuum*, *J. Opt. Soc. Am. B* **1**, 169-175 (1984); A. K. Kazansky, *Precise analysis of resonance decay law in atomic physics*, *J. Phys. B: At. Mol. Opt. Phys.* **30**, 1404-1410 (1997); N. Shenvi, J. R. Schmidt, S. T. Edwards, and J. C. Tully, *Efficient discretization of the continuum through complex contour deformation*, *Phys. Rev. A* **78**, 022502 (2008).
- [17] R. Bulla, Th. Pruschke, and A. C. Hewson, *Anderson impurity in pseudo-gap Fermi systems*, *J. Phys. Condens. Matter* **9**, 10463-10474 (1997).
- [18] Herbert S. Wilf, *Mathematics for the Physical Sciences*, Dover Publication, inc. (New York, 1962).
- [19] W. Gautschi, G. V. Milovanović, *Polynomials orthogonal on the Semicircle*, *J. Approx. Theo.* **46**, 230-250 (1986); W. Gautschi, H. J. Landau, and G. V. Milovanović, *Polynomials orthogonal on the Semicircle II*, *Constr. Approx.* **3**, 389-404 (1987).
- [20] Dorje C Brody, *Biorthogonal quantum mechanics*, *J. Phys. A: Math. Theo.* **47**, 035305 (2014).
- [21] D. A. Abanin, E. Altman, I. Bloch, and M. Serbyn, *Colloquium: many-body localization, thermalization, and entanglement*, *Rev. Mod. Phys.* **91**, 021001 (2019).
- [22] S. Aubry and G. André, *Analyticity Breaking and Anderson Localization in Incommensurate Lattices*, *Ann. Isr. Phys. Soc.* **3**, 33 (1980); P. G. Haper, *Single Band Motion of Conduction Electrons in a Uniform Magnetic Field*, *Proc. Phys. Soc. London Sect. A* **68**, 874 (1955).
- [23] E. Levi, M. Heyl, I. Lesanovsky, and J. P. Garrahan, *Robustness of many-body localization in the presence of dissipation*, *Phys. Rev. Lett.* **116**, 237203 (2016); M. H. Fischer, M. Maksymenko, and E. Altman, **116**, 160401 (2016); H. P. Lüschen, P. Bordia, S. S. Hodgman, M. Schrieber, S. Sarkar, A. J. Daley, M. H. Fischer, E. Altman, I. Bloch, and U. Schneider, *Signature of many-body localization in a controlled open quantum system*, *Phys. Rev. X* **7**, 011034 (2017).
- [24] E. M. Kessler, G. Giedke, A. Imamoglu, S. F. Yelin, M. D. Lukin, and J. I. Cirac, *Dissipative phase transition in a central spin system*, *Phys. Rev. A* **86**, 012116 (2012).
- [25] I. Rotter, *A non-Hermitian Hamilton operator and the physics of open quantum systems*, *J. Phys. A: Math. Theor.* **42**, 153001 (2009).
- [26] B. M. Garraway, *Nonperturbative decay of an atomic system in a cavity*, *Phys. Rev. A* **55**, 2290-2303 (1996); D. Tamascelli, A. Smirne, S. F. Huelga, and M. B. Plenio, *Phys. Rev. Lett.* **120**, 030402 (2018); N. Lambert, S. Ahmed, M. Cirio, and F. Nori, *Nat. Commun.* **10**, 3721 (2019); S. Xu, H. Z. Shen, X. X. Yi, and W. Wang, *Readout of the spectral density of an environment from the dynamics of an open system*, *Phys. Rev. A* **100**, 032108 (2019); G. Pleasance, B. M. Garraway, and F. Petruccione, *Generalized theory of pseudomodes for exact description of non-Markovian quantum processes*, *Phys. Rev. Res.* **2**, 043058 (2020); G. Pleasance, F. Petruccione, *Pseudomode description of general open quantum system dynamics: non-perturbative master equation for the spin-boson model*, arXiv: 2108.05755 [quant-ph] (2021).
- [27] A. G. Kofman, G. Kurizki, and B. Sherman, *Spontaneous and induced atomic decay in photonic band structures*, *J. Mod. Opt.* **41**, 353-384 (1994).
- [28] Q.-J. Tong, J.-H. An, H.-G. Luo, and C. H. Oh, *Mechanism of entanglement preservation*, *Phys. Rev. A* **81**, 052330 (2010); H.-N. Xiong, W.-M. Zhang, Xiaoguang Wang, and M.-H. Wu, *Exact non-Markovian cavity dynamics strongly coupled a reservoir*, *Phys. Rev. A* **82**, 012105 (2010); Q.-J. Tong, J.-H. An, H.-G. Luo, and C. H. Oh, *Quantum phase transition in the delocalized regime of the spin-boson model*, *Phys. Rev. B* **84**, 174301 (2011).